A Novel 3D Regular-Shaped Geometry-Based Stochastic Model for Non-Isotropic MIMO Mobile-to-Mobile Channels

(Invited Paper)

Xiang Cheng[1], Cheng-Xiang Wang[1], Yi Yuan[1], David I. Laurenson[2], and Xiaohu Ge[3]

[1]Joint Research Institute for Signal and Image Processing, Heriot-Watt University, Edinburgh EH14 4AS, UK.

[2]Joint Research Institute for Signal and Image Processing, University of Edinburgh, Edinburgh EH9 3JL, UK.

[3]Department of Electronics and Information Engineering, Huazhong University of Science and Technology, Wuhan 430074, P. R. China.

Email: xiangcheng.86@googlemail.com, cheng-xiang.wang@hw.ac.uk, yy120@hw.ac.uk, dave.laurenson@ed.ac.uk, xhge@mail.hust.edu.cn

***Abstract*—This paper proposes a novel three-dimensional (3D) regular-shaped geometry-based stochastic model (RS-GBSM) for non-isotropic multiple-input multiple-output (MIMO) mobile-to-mobile (M2M) Ricean fading channels. The proposed model, combining a two-sphere model and an elliptic-cylinder model, is the first 3D RS-GBSM that has the ability to investigate the impact of the vehicular traffic density (VTD) on channel statistics and jointly consider the azimuth angle and elevation angle. From the proposed model, the space-time (ST) correlation function (CF) and the corresponding space-Doppler (SD) power spectral density (PSD) are derived. Finally, some numerical results and interesting observations are given.**

I. Introduction

In vehicular ad hoc networks (VANETs), intelligent transportation systems, and cooperative systems [1], M2M communications are often encountered that require the direct communication between two moving stations both equiped with low elevation antennas. M2M channel modeling is of great importance for the successful design and performance assessment of such M2M communication systems. In [2], the existing M2M channel models were classified and future challenges were identified. Among all the available M2M channel models, RS-GBSMs are the most widely used that assume that the effective scatterers are static and located on a regular geometric shape, e.g., one-ring, two-ring, or ellipse in two-dimentional (2D) cases. In [3] and [4], the authors proposed a 2D two-ring RS-GBSM for isotropic single-input single-output (SISO) M2M Rayleigh fading channels. In [5], a 2D two-ring RS-GBSM was presented for non-isotropic MIMO M2M Ricean fading channels. Recently, narrowband and wideband 2D RS-GBSMs, combining a two-ring model and an ellipse(s) model, were proposed for non-isotropic MIMO M2M Ricean fading channels in [6] and [7], respectively.

All the above mentioned RS-GBSMs are 2D M2M channel models, which assume that waves travel only in the horizontal plane. This assumption omits signal variations in the vertical plane and is valid only when the transmitter (Tx) and receiver (Rx) are sufficiently separated. In reality, waves do travel in three dimentions. Therefore, it is desirable to develop more realistic 3D M2M channel models that consider both azimuth and elevation angles. To the best of the authors' knowledge, only two 3D M2M RS-GBSMs are currently available: a narrowband 3D two-cylinder RS-GBSM in [8] and a corresponding wideband 3D two-concentric-cylinder RS-GBSM in [9] for non-isotropic MIMO M2M channels. However, both the aforementioned 3D RS-GBSMs assumed that the azimuth and elevation angles are completely independent. This assumption differs from reality and thus reduces the accuracy of these models. Furthermore, although the measurement campaigns in [10] and [11] and theoretical results in [6] and [7] have demonstrated that the VTD significantly affects the channel statistics of M2M channels, the impact of the VTD was not considered in the existing 3D RS-GBSMs in [8] and [9].

To fill the above gap, this paper proposes a novel 3D RS-GBSM for non-isotropic narrowband MIMO M2M Ricean fading channels. This 3D model comprises a single- and double-bounce two-sphere model, a single-bounce elliptic-cylinder model, and line-of-sight (LoS) components, thus having the ability to adapt to a wide variety of scenarios. By applying the von Mises-Fisher (VMF) distribution [12] as the scatterer distribution, the proposed model can jointly consider the azimuth and elevation angles. In order to take into account the impact of the VTD on channel statistics in the proposed 3D model, we use a two-sphere model to describe moving scatterers and an elliptic-cylinder model to represent stationary scatterers. From the proposed model, we further derive the ST CF and the corresponding SD PSD. Finally, some numerical results are shown and interesting observations are given.

The remainder of this paper is outlined as follows. Section II presents a novel 3D RS-GBSM for non-isotropic narrowband MIMO M2M Ricean fading channels. In Section III, from the proposed model, we derive the ST CF and the corresponding SD PSD. Numerical results and analysis are presented in Section IV. Finally, conclusions are drawn in Section V.

II. A Novel 3D MIMO M2M RS-GBSM

This paper considers a narrrowband MIMO M2M communication system with M_T transmit and M_R receive omni-directional antenna elements. Both the Tx and Rx are equipped with low elevation antennas. Fig. 1 illustrates the proposed 3D RS-GBSM, which is the combination of a single- and double-bounce two-sphere model, a single-bounce elliptic-cylinder model, and LoS components. For readability purposes, Fig. 1 only shows the geometry of the single-bounce elliptic-cylinder

978-1-4244-3574-6/10/$25.00 ©2010 IEEE

model and LoS components. The detailed geometry of the single- and double-bounce two-sphere model is given in Fig. 2. Note that in Figs. 1 and 2, we used uniform linear antenna arrays with M_T=M_R=2 as an example. The proposed model is applicable to MIMO systems with arbitrary numbers of antenna elements. The two-sphere model defines two spheres of effective scatterers, one around the Tx and the other around the Rx. Suppose there are N_1 effective scatterers around the Tx lying on a sphere of radius R_T and the n_1th (n_1=$1, ..., N_1$) effective scatterer is denoted by $s^{(n_1)}$. Similarly, assume there are N_2 effective scatterers around the Rx lying on a sphere of radius R_R and the n_2th (n_2=$1, ..., N_2$) effective scatterer is denoted by $s^{(n_2)}$. For the elliptic-cylinder model, N_3 effective scatterers lie on an elliptic-cylinder with the Tx and Rx located at the foci and the n_3th ($n_3 = 1, ..., N_3$) effective scatterer is denoted by $s^{(n_3)}$. The parameters in Figs. 1 and 2 are defined in Table I. Note that the reasonable assumptions $D \gg \max\{R_T, R_R\}$ and $\min\{R_T, R_R, a-f\} \gg \max\{\delta_T, \delta_R\}$ [6] are applied in the proposed model.

The MIMO fading channel can be described by a matrix $\mathbf{H}(t) = [h_{pq}(t, \tau')]_{M_R \times M_T}$ of size $M_R \times M_T$. The received complex fading envelope between the pth ($p = 1, ..., M_T$) Tx and the qth ($q = 1, ..., M_R$) Rx at the carrier frequency f_c is a superposition of the LoS, single-, and double-bounced components, and can be expressed as [6]

$$h_{pq}(t) = h_{pq}^{LoS}(t) + \sum_{i=1}^{I} h_{pq}^{SB_i}(t) + h_{pq}^{DB}(t) \tag{1}$$

where

$$\begin{aligned} h_{pq}^{LoS}(t) &= \sqrt{\frac{K}{K+1}} e^{j2\pi f_{T_{max}} t \cos\left(\alpha_T^{LoS} - \gamma_T\right) \cos \beta_T^{LoS}} \\ &\times e^{-j2\pi f_c \tau_{pq}} e^{2\pi f_{R_{max}} t \cos\left(\alpha_R^{LoS} - \gamma_R\right) \cos \beta_R^{LoS}} \quad (2a) \\ h_{pq}^{SB_i}(t) &= \sqrt{\frac{\eta_{SB_i}}{K+1}} \lim_{N_i \to \infty} \sum_{n_i=1}^{N_i} \frac{1}{\sqrt{N_i}} e^{j\left(\psi_{n_i} - 2\pi f_c \tau_{pq,n_i}\right)} \\ &\times e^{j2\pi f_{T_{max}} t \cos\left(\alpha_T^{(n_i)} - \gamma_T\right) \cos \beta_T^{(n_i)}} \\ &\times e^{j2\pi f_{R_{max}} t \cos\left(\alpha_R^{(n_i)} - \gamma_R\right) \cos \beta_R^{(n_i)}} \quad (2b) \\ h_{pq}^{DB}(t) &= \sqrt{\frac{\eta_{DB}}{K+1}} \lim_{N_1, N_2 \to \infty} \sum_{n_1, n_2 = 1}^{N_1, N_2} \frac{1}{\sqrt{N_1 N_2}} e^{j\psi_{n_1, n_2}} \\ &\times e^{j2\pi f_c \tau_{pq,n_1,n_2}} e^{j2\pi f_{T_{max}} t \cos\left(\alpha_T^{(n_1)} - \gamma_T\right) \cos \beta_T^{(n_1)}} \\ &\times e^{2\pi f_{R_{max}} t \cos\left(\alpha_R^{(n_2)} - \gamma_R\right) \cos \beta_R^{(n_2)}} \quad (2c) \end{aligned}$$

with $\alpha_T^{LoS} \approx \beta_T^{LoS} \approx \beta_R^{LoS} \approx 0$, $\alpha_R^{LoS} \approx \pi$, $\tau_{pq} = \varepsilon_{pq}/c$, $\tau_{pq,n_i} = (\varepsilon_{pn_i} + \varepsilon_{n_i q})/c$, and $\tau_{pq,n_1,n_2} = (\varepsilon_{pn_1} + \varepsilon_{n_1 n_2} + \varepsilon_{n_2 q})/c$. Here, c is the speed of light, K designates the Ricean factor, and I=3. Power-related parameters η_{SB_i} and η_{DB} specify the amount of powers that the single- and double-bounced rays contribute to the total scattered power $1/(K+1)$. Note that these power-related parameters satisfy $\sum_{i=1}^{I} \eta_{SB_i} + \eta_{DB} = 1$. The phases ψ_{n_i} and ψ_{n_1,n_2} are independent and identically distributed (i.i.d.) random variables with uniform distributions over $[-\pi, \pi)$, $f_{T_{max}}$ and $f_{R_{max}}$ are the maximum Doppler frequencies with respect to the Tx and Rx, respectively. Note that in order to significantly reduce the complexity of the proposed model, only the double-bounced rays via scatterers on the two-sphere model are considered as the other double-bounced rays (via one scatter on a sphere and the other one on the elliptic-cylinder) show similar channel statistics.

As addressed in [6], [7] [10], and [11], the VTD significantly affects statistical properties of M2M channels. To take the impact of the VTD into account, we distinguish between the moving scatterers (cars) around the Tx and Rx, and stationary scatterers located on the roadside (e.g., buildings, bridges, trees, etc.), which are described by the two-sphere model and the elliptic-cylinder model, respectively. For a low VTD scenario, K is large since the LoS component can bear a significant amount of power. Also, the received scattered power is mainly from waves reflected by the stationary scatterers located on the elliptic-cylinder. The moving scatterers located on the two spheres are sparse and thus more likely to be single-bounced, rather than double-bounced. This indicates that $\eta_{SB_3} > \max\{\eta_{SB_1}, \eta_{SB_2}\} > \eta_{DB}$. For a high VTD scenario, K is smaller than the one in a low VTD scenario. Also, due to the large amount of moving scatterers, the double-bounced rays of the two-sphere model bear more power than single-bounced rays of two-sphere and elliptic-cylinder models, i.e., $\eta_{DB} > \max\{\eta_{SB_1}, \eta_{SB_2}, \eta_{SB_3}\}$.

From Figs. 1 and 2 and applying the law of cosines in appropriate triangles and small angle approximations (i.e., $\sin x \approx x$ and $\cos x \approx 1$ for small x), we have

$$\begin{aligned} \varepsilon_{pq} &\approx \xi - \frac{\delta_R}{2\xi}\left[\frac{\delta_T}{2} \sin\varphi_T \sin\varphi_R - Q \cos\varphi_R \cos\theta_R\right] \quad (3a) \\ \varepsilon_{pn_1} &\approx R_T - \frac{\delta_T}{2}\left[\sin\beta_T^{(n_1)} \sin\varphi_T + \cos\beta_T^{(n_1)}\right. \\ &\times \left.\cos\varphi_T \cos(\theta_T - \alpha_T^{(n_1)})\right] \quad (3b) \\ \varepsilon_{n_1 q} &\approx \xi_{n_1} - \frac{\delta_R}{2\xi_{n_1}}\left[R_T \sin\beta_T^{(n_1)} \sin\varphi_R\right. \\ &- \left. Q_{n_1} \cos\varphi_R \cos(\alpha_R^{(n_1)} - \theta_R)\right] \quad (3c) \\ \varepsilon_{pn_2} &\approx \xi_{n_2} - \frac{\delta_T}{2\xi_{n_2}}\left[R_R \sin\beta_R^{(n_2)} \sin\varphi_T\right. \\ &+ \left. Q_{n_2} \cos\varphi_T \cos(\alpha_T^{(n_2)} - \theta_T)\right] \quad (3d) \\ \varepsilon_{n_2 q} &\approx R_R - \frac{\delta_R}{2}\left[\sin\beta_R^{(n_2)} \sin\varphi_R + \cos\beta_R^{(n_2)}\right. \\ &\times \left.\cos\varphi_R \cos(\theta_R - \alpha_R^{(n_2)})\right] \quad (3e) \\ \varepsilon_{n_1 n_2} &\approx \left\{\left[D - R_T \cos\alpha_T^{(n_1)} - R_R \cos(\alpha_R^{(n_1)} - \alpha_R^{(n_2)})\right]^2\right. \\ &+ \left.\left[R_T \cos\beta_T^{(n_1)} - R_R \cos\beta_R^{(n_2)}\right]^2\right\}^{1/2} \quad (3f) \\ \varepsilon_{pn_3} &\approx \xi_T^{(n_3)} - \frac{\delta_T}{2\xi_T^{(n_3)}}\left[\xi_R^{(n_3)} \sin\beta_R^{(n_3)} \sin\varphi_T\right. \\ &+ \left. Q_{n_3} \cos\varphi_T \cos(\alpha_T^{(n_3)} - \theta_T)\right] \quad (3g) \\ \varepsilon_{n_3 q} &\approx \xi_R^{(n_3)} - \delta_R\left[\sin\beta_R^{(n_3)} \sin\varphi_R\right. \\ &+ \left. \cos\beta_R^{(n_3)} \cos\varphi_R \cos(\alpha_R^{(n_3)} - \theta_R)\right] \quad (3h) \end{aligned}$$

where $\xi \approx Q \approx D - \delta_T \cos\varphi_T \cos\theta_T/2$, $\xi_{n_1} = \left[Q_{n_1}^2 + R_T^2\right.$

$\times \sin^2\beta_T^{(n_1)}\Big]^{1/2}$, $Q_{n_1} \approx D - R_T\cos\beta_T^{(n_1)}\cos\alpha_T^{(n_1)}$, $\xi_{n_2} = \Big[Q_{n_2}^2 + R_R^2\sin^2\beta_R^{(n_2)}\Big]^{1/2}$, $Q_{n_2} \approx D + R_R\cos\beta_R^{(n_2)}\cos\alpha_R^{(n_2)}$, $\xi_T^{(n_3)} = \Big[Q_{n_3}^2 + (\xi_R^{(n_3)})^2\sin^2\beta_R^{(n_3)}\Big]^{1/2}$, $\xi_R^{(n_3)} = (2a - Q_{n_3})/\cos\beta_R^{(n_3)}$, and $Q_{n_3} = (a^2+f^2+2af\cos\alpha_R^{(n_3)})/(a + f\cos\alpha_R^{(n_3)})$. The derivations in (3a)–(3h) are complicated and lengthy. Details are omitted here for brevity. Note that the azimuth angle of departure (AAoD) $\alpha_T^{(n_i)}$ and azimuth angle of arrival (AAoA) $\alpha_R^{(n_i)}$ are independent for double-bounced rays, while are interdependent for single-bounced rays. By using the results in [6], for the single-bounce two-sphere model we can express the relationship between the AAoD and AAoA as $\alpha_R^{(n_1)} \approx \pi - \Delta_T\sin\alpha_T^{(n_1)}$ and $\alpha_T^{(n_2)} \approx \Delta_R\sin\alpha_R^{(n_2)}$ with $\Delta_T \approx R_T/D$ and $\Delta_R \approx R_R/D$. For the elliptic-cylinder model, $\alpha_T^{(n_3)} = \arcsin[b^2\sin\alpha_R^{(n_3)}/(a^2+f^2+2af\cos\alpha_R^{(n_3)})]$ holds with b denoting the semi-minor axis of the elliptic-cylinder.

Since the numbers of effective scatterers are assumed to be infinite, i.e., $N_i \to \infty$, the proposed model is actually a mathematical reference model and results in Ricean probability distribution function (PDF). For our reference model, the discrete AAoD $\alpha_T^{(n_i)}$, elevation AoD (EAoD) $\beta_T^{(n_i)}$, AAoA $\alpha_R^{(n_i)}$, and elevation AoA (EAoA) $\beta_R^{(n_i)}$ can be replaced by continuous random variables $\alpha_T^{(i)}$, $\beta_T^{(i)}$, $\alpha_R^{(i)}$, and $\beta_R^{(i)}$, respectively. In order to jointly consider the impact of the azimuth and elevation angles on channel statistics, we use the VMF PDF to characterize the distribution of effective scatterers. The VMF PDF is defined as [12] $f(\alpha,\beta) \triangleq \frac{k}{4\pi\sinh k}\exp\{k[\cos\beta_0\cos\beta\cos(\alpha-\alpha_0)+\sin\beta_0\sin\beta]\}\cos\beta$, where $\alpha,\beta\in[-\pi,\pi)$, $\alpha_0\in[-\pi,\pi)$ and $\beta_0\in[-\pi,\pi)$ account for the mean values of the azimuth angle α and elevation angle β, respectively, and k ($k\geq 0$) is a real-valued parameter that controls the concentration of the distribution relative to the mean direction identified by α_0 and β_0. The larger the value of k, the more concentrated towards the mean direction the distribution is. For $k=0$ the distribution is isotropic, while for $k=\infty$ the distribution becomes extremely non-isotropic. Note that when the elevation angle $\beta = 0$, the VMF PDF reduces to von Mises PDF, which is widely applied as a scatterer distribution in 2D propagation environments [13]. In this paper, for the angles of interest, e.g., the AAoD $\alpha_T^{(1)}$ and EAoD $\beta_T^{(1)}$ for the Tx sphere, the AAoA $\alpha_R^{(2)}$ and EAoA $\beta_R^{(2)}$ for the Rx sphere, and the AAoA $\alpha_R^{(3)}$ and EAoA $\beta_R^{(3)}$ for the elliptic-cylinder, the parameters (α_0, β_0 and k) of the VMF PDF are denoted by $\alpha_{T0}^{(1)}$, $\beta_{T0}^{(1)}$ and $k^{(1)}$, $\alpha_{R0}^{(2)}$, $\beta_{R0}^{(2)}$ and $k^{(2)}$, and $\alpha_{R0}^{(3)}$, $\beta_{R0}^{(3)}$ and $k^{(3)}$, respectively.

III. ST CF AND SD PSD

In this section, based on the proposed 3D channel model, we will derive the ST CF and the corresponding SD PSD for a non-isotropic scattering environment.

Under the wide-sense stationary (WSS) condition, the normalized ST CF between any two complex fading envelopes $h_{pq}(t)$ and $h_{p'q'}(t)$ is defined as [6] $\rho_{h_{pq}h_{p'q'}}(\tau) = \mathbf{E}\left[h_{pq}(t)\,h_{p'q'}^*(t-\tau)\right](1+K)$, where $(\cdot)^*$ denotes the complex conjugate operation and $\mathbf{E}[\cdot]$ designates the statistical expectation operator. Substituting the proposed model in (1) into the above defined CF and applying the corresponding VMF distribution, we can obtain the ST CF of the LoS, single-, and double-bounced components as follows.

1) In the case of the LoS component,

$$\rho_{h_{pq}^{LoS}h_{p'q'}^{LoS}}(\tau) = Ke^{\frac{j2\pi}{\lambda}A^{LoS}+j2\pi\tau(f_{T_{max}}\cos\gamma_T - f_{R_{max}}\cos\gamma_R)} \quad (4)$$

where $A^{LoS} = 2D\cos\varphi_R\cos\theta_R$.

2) In terms of the single-bounce two-sphere model

$$\rho_{h_{pq}^{SB_{1(2)}}h_{p'q'}^{SB_{1(2)}}}(\tau) = \eta_{SB_{1(2)}}\int_{-\pi}^{\pi}\int_{-\pi}^{\pi}\frac{k^{(1(2))}\cos\beta_{T(R)}^{(1(2))}}{4\pi\sinh k^{(1(2))}}e^{\frac{j2\pi}{\lambda}A^{(1(2))}}$$
$$e^{k^{(1(2))}[\cos\beta_{T(R)0}^{(1(2))}\cos\beta_{T(R)}^{(1(2))}\cos(\alpha_{T(R)}^{(1(2))}-\alpha_{T(R)0}^{(1(2))})+\sin\beta_{T(R)0}^{(1(2))}\sin\beta_{T(R)}^{(1(2))}]}$$
$$e^{j2\pi\tau(f_{T_{max}}B^{(1(2))}+f_{R_{max}}C^{(1(2))})}d\alpha_{T(R)}^{(1(2))}d\beta_{T(R)}^{(1(2))} \quad (5)$$

with $A^{(1(2))} = \delta_{T(R)}[\sin\beta_{T(R)}^{(1(2))}\sin\varphi_{T(R)} + \cos\beta_{T(R)}^{(1(2))}\cos\varphi_{T(R)}\times\cos(\theta_{T(R)} - \alpha_{T(R)}^{(1(2))})] + \frac{\delta_{R(T)}}{\xi_{n_{1(2)}}}[R_{T(R)}\sin\beta_{T(R)}^{(1(2))}\sin\varphi_{R(T)} \mp Q_{n_{1(2)}}\cos\varphi_{R(T)}\cos(\theta_{R(T)} - \alpha_{R(T)}^{(2(1))})]$, $B^{(1(2))} = \cos(\alpha_T^{(1)}(\Delta_R\sin\alpha_R^{(2)}) - \gamma_T)\cos(\beta_T^{(1)}(\arccos\frac{D+R_R\cos\beta_R^{(2)}\cos\alpha_R^{(2)}}{\xi_{n_2}}))$, and $C^{(2(1))} = \cos(\alpha_R^{(2)}(\pi - \Delta_T\sin\alpha_T^{(1)}) - \gamma_R)\cos(\beta_R^{(2)}(\arccos\frac{D - R_T\cos\beta_T^{(1)}\cos\alpha_T^{(1)}}{\xi_{n_1}}))$, where the expressions of $Q_{n_{1(2)}}$ and $\xi_{n_{1(2)}}$ are given after (3h) in Section II.

3) In the case of the single-bounce elliptic-cylinder model

$$\rho_{h_{pq}^{SB_3}h_{p'q'}^{SB_3}}(\tau) = \eta_{SB_3}\int_{-\pi}^{\pi}\int_{-\pi}^{\pi}\frac{k^{(3)}\cos\beta_R^{(3)}}{4\pi\sinh k^{(3)}}e^{\frac{j2\pi}{\lambda}A^{(3)}}$$
$$e^{k^{(3)}[\cos\beta_{R0}^{(3)}\cos\beta_R^{(3)}\cos(\alpha_R^{(3)}-\alpha_{R0}^{(3)})+\sin\beta_{R0}^{(3)}\sin\beta_R^{(3)}]}$$
$$e^{j2\pi\tau(f_{T_{max}}B^{(3)}+f_{R_{max}}C^{(3)})}d\alpha_R^{(3)}d\beta_R^{(3)} \quad (6)$$

with $A^{(3)} = \frac{\delta_T}{\xi_T^{(n_3)}}[\xi_R^{(n_3)}\sin\beta_R^{(3)}\sin\varphi_T + Q_{n_3}\cos\varphi_T\cos(\theta_T - \alpha_T^{(3)})] + \delta_R[\sin\beta_R^{(3)}\sin\varphi_R + \cos\beta_R^{(3)}\cos\varphi_R\cos(\theta_R - \alpha_R^{(3)})]$, $B^{(3)} = \cos(\alpha_T^{(3)} - \gamma_T)\cos\beta_T^{(3)}$, $C^{(3)} = \cos(\alpha_R^{(3)} - \gamma_R)\cos\beta_R^{(3)}$, and $\beta_T^{(3)} = \arccos\frac{a^2+f^2+2af\cos\alpha_R^{(3)}}{(a+f\cos\alpha_R^{(3)})\xi_T^{n_3}}$, where the expressions of Q_{n_3}, $\xi_{T(R)}^{n_3}$, and $\alpha_T^{(3)}$ are given after (3h) in Section II.

4) In terms of the double-bounce two-sphere model

$$\rho_{h_{pq}^{DB}h_{p'q'}^{DB}}(\tau) = \rho_{pp}^T(\tau)\,\rho_{qq}^R(\tau) = \eta_{DB}\int_{-\pi}^{\pi}\int_{-\pi}^{\pi}\int_{-\pi}^{\pi}\int_{-\pi}^{\pi}\frac{k^{(1)}k^{(2)}\cos\beta_R^{(1)}}{8\pi^2\sinh k^{(1)}}$$
$$\frac{\cos\beta_R^{(2)}}{\sinh k^{(2)}}e^{k^{(1)}[\cos\beta_{T0}^{(1)}\cos\beta_T^{(1)}\cos(\alpha_T^{(1)}-\alpha_{T0}^{(1)})+\sin\beta_{T0}^{(1)}\sin\beta_T^{(1)}]}$$
$$e^{\frac{j2\pi}{\lambda}A^{DB}}e^{k^{(2)}[\cos\beta_{R0}^{(2)}\cos\beta_R^{(2)}\cos(\alpha_R^{(2)}-\alpha_{R0}^{(2)})+\sin\beta_{R0}^{(2)}\sin\beta_R^{(2)}]}$$
$$e^{j2\pi\tau(f_{T_{max}}B^{DB}+f_{R_{max}}C^{DB})}d\alpha_T^{(1)}d\beta_T^{(1)}d\alpha_R^{(2)}d\beta_R^{(2)} \quad (7)$$

where $A^{DB} = \delta_T[\sin\beta_T^{(1)}\sin\varphi_T + \cos\beta_T^{(1)}\cos\varphi_T\cos(\theta_T - \alpha_T^{(1)})] + \delta_R[\sin\beta_R^{(2)}\sin\varphi_R + \cos\beta_R^{(2)}\cos\varphi_R\cos(\theta_R - \alpha_R^{(2)})]$, $B^{DB} = \cos(\alpha_T^{(1)} - \gamma_T)\cos\beta_T^{(1)}$, and $C^{DB} = \cos(\alpha_R^{(2)} - \gamma_R)\cos\beta_R^{(2)}$.

Finally, the normalized ST CF $\rho_{h_{pq}h_{p'q'}}(\tau)$ can be expressed as the summation of (4)–(7).

Applying the Fourier transform to the ST CF $\rho_{h_{pq}h_{p'q'}}(\tau)$ in terms of τ, we can obtain the corresponding SD PSD as $S_{h_{pq}h_{p'q'}}(f_D) = F\left\{\rho_{h_{pq}h_{p'q'}}(\tau)\right\} = \int_{-\infty}^{\infty} \rho_{h_{pq}h_{p'q'}}(\tau)\, e^{-j2\pi f_D \tau} d\tau$, where f_D is the Doppler frequency. Substituting (4)–(7) into the above defined SD PSD, we have $S_{h_{pq}h_{p'q'}}(f_D) = F\left\{\rho_{h_{pq}^{LoS}h_{p'q'}^{LoS}}(\tau)\right\} + \sum_{i=1}^{I} F\left\{\rho_{h_{pq}^{SB_i}h_{p'q'}^{SB_i}}(\tau)\right\} + F\left\{\rho_{pp'}^{T}(\tau)\right\} \odot F\left\{\rho_{qq'}^{R}(\tau)\right\}$, where $\odot$ denotes the convolution. Due to the page limit, detailed expressions of the SD PSD are omitted here.

IV. Numerical Results and Analysis

The following parameters are used for our numerical analysis: $f_c = 5.9$ GHz, $f_{T_{max}} = f_{R_{max}} = 570$ Hz, $D = 300$ m, a=180 m, and R_T=R_R=15 m.

Fig. 3 shows the SD PSDs of the proposed 3D MIMO M2M RS-GBSM with different VTDs and different antenna separations (δ_T=δ_R=0 or δ_T=δ_R=3λ) when the Tx and Rx move in the same direction (γ_T=γ_R=0°). Note that when δ_T=δ_R=0, the SD PSDs actually reduce to Doppler PSDs. For a low VTD scenario, we choose the following environment-related parameters: $k^{(1)} = 9.6$, $k^{(2)} = 3.6$, $k^{(3)} = 11.5$, $\alpha_{T0}^{(1)} = 21.7°$, $\alpha_{R0}^{(2)} = 147.8°$, $\alpha_{R0}^{(3)} = 171.6°$, $\beta_{T0}^{(1)} = 6.7°$, $\beta_{R0}^{(2)} = 17.2°$, $\beta_{R0}^{(3)}$=31.6°. Considering the constraints of the Ricean factor and power-related parameters as mentioned in Section II, we have the following parameters for the low VTD scenario: $K = 3.786$, $\eta_{DB} = 0.051$, $\eta_{SB_1} = 0.335$, $\eta_{SB_2} = 0.203$, and η_{SB_3}=0.411. The environment-related parameters for the high VTD scenario are the same as those for the low VTD scenario except $k^{(1)} = 0.6$ and $k^{(2)} = 1.3$, which are related to the distribution of moving scatterers (normally, the smaller values the more distributed moving scatterers, i.e., the higher VTD). The SD PSDs for high VTD shown in Fig. 3 are obtained with the following parameters $K = 0.156$, $\eta_{DB} = 0.685$, η_{SB_1}=η_{SB_2}=0.126, η_{SB_3}=0.063. Comparing the SD PSDs with different VTDs in Fig. 3, we observe that the VTD significantly affects the SD PSD of M2M channels. The higher the VTD, the more evenly distributed the (space-)Doppler PSD is. The underlying physical explanation is that compared to the lower VTD scenario, where the received power mainly comes from several directions identified by main stationary roadside scatterers (e.g., large buildings, bridge, etc.) and LoS components, the higher VTD scenario has the received power coming from all directions scattered by moving cars around the Tx and Rx. Moreover, the space separation results in the fluctuations on SD PSDs. For comparison purposes, the Doppler PSDs of the 2D RS-GBSM obtained from the proposed 3D RS-GBSM by setting $\beta_T^{(n_1)}$=$\beta_R^{(n_2)}$=$\beta_R^{(n_3)}$=0° are also plotted in Fig. 3. It is clear that no matter what the VTD is, the Doppler PSD of the 2D model is more distributed than that of the 3D model. This means that the 2D model underestimates the Doppler PSD, i.e., a M2M channel varies faster than estimated by the 2D model.

By using the same parameters as in Fig. 3, Fig. 4 depicts the space CFs. Again, the VTD significantly affects the space CFs. Higher VTDs lead to lower correlation properties. This is because the higher the VTD, the more spatial diversity the M2M channel has. Furthermore, Fig. 4 also shows that the 2D model (i.e., $\beta_T^{(n_1)}$=$\beta_R^{(n_2)}$=$\beta_R^{(n_3)}$=0°) overestimates the spatial correlations, i.e., underestimates the spatial diversity gain. This is because the vertically spatial diversity gain cannot be modeled by the 2D model.

V. Conclusions

In this paper, we have proposed a novel 3D MIMO M2M RS-GBSM that has the ability to investigate the impact of the VTD and the joint impact of the azimuth and elevation angles on channel statistics. From the proposed 3D model, the ST CFs and SD PSDs have been derived. Numerical results have demonstrated that the VTD has a great impact on the resulting CFs and PSDs. Finally, it has been shown that the reduced 2D model underestimates both the temporal and spatial diversity gains, which highlights the necessity of developing 3D M2M channel models.

To further validate the utility of the proposed 3D reference model, our future work will be devoted to comparing the statistical properties of the proposed model with measurement data, e.g., in [8]. Moreover, a corresponding 3D MIMO M2M simulation model will be developed, as an extension to the 2D M2M simulation models in [14].

Acknowledgments

The authors acknowledge the support from the RCUK for the UK-China Science Bridges Project: R&D on (B)4G Wireless Mobile Communications. X. Cheng, C.-X. Wang, Y. Yuan, and D. I. Laurenson acknowledge the support from the Scottish Funding Council for the Joint Research Institute in Signal and Image Processing, as part of the Edinburgh Research Partnership in Engineering and Mathematics (ERPem). X. Ge also acknowledges the support from the National Natural Science Foundation of China (NSFC) (contract/grant number: 60872007), National 863 High Technology Program of China (contract/grant number: 2009AA01Z239), and Ministry of Science and Technology (MOST) of China for the International Science and Technology Collaboration Program (contract/grant number: 0903).

References

[1] C.-X. Wang, X. Hong, X. Ge, X. Cheng, G. Zhang, and J. S. Thompson, "Cooperative MIMO channel models: a survey," *IEEE Commun. Mag.*, vol. 48, no. 2, pp. 80–87, Feb. 2010.

[2] C.-X. Wang, X. Cheng, and D. I. Laurenson, "Vehicle-to-vehicle channel modeling and measurements: recent advances and future challenges," *IEEE Commun. Mag.*, vol. 47, no. 11, pp. 96–103, Nov. 2009.

[3] A. S. Akki and F. Haber, "A statistical model for mobile-to-mobile land communication channel," *IEEE Trans. Veh. Technol.*, vol. 35, no. 1, pp. 2–10, Feb. 1986.

[4] A. S. Akki, "Statistical properties of mobile-to-mobile land communication channels," *IEEE Trans. Veh. Technol.*, vol. 43, no. 4, pp. 826–831, Nov. 1994.

[5] A. G. Zajić and G. L. Stüber, "Space-time correlated mobile-to-mobile channels: modelling and simulation," *IEEE Trans. Veh. Technol.*, vol. 57, no. 2, pp. 715–726, Mar. 2008.

[6] X. Cheng, C.-X. Wang, D. I. Laurenson, S. Salous, and A. V. Vasilakos, "An adaptive geometry-based stochastic model for non-isotropic MIMO mobile-to-mobile channels," *IEEE Trans. Wireless Commun.*, vol. 8, no. 9, pp. 4824–4835, Sept. 2009.

[7] X. Cheng, C.-X. Wang, and D. I. Laurenson, "A Geometry-based stochastic model for wideband MIMO mobile-to-mobile channels," *Proc. IEEE GLOBECOM'09*, Hawaii, USA, Nov.–Dec. 2009.

[8] A. G. Zajić and G. L. Stüber, "Three-dimensional modeling, simulation, and capacity analysis of space-time correlated mobile-to-mobile channels," *IEEE Trans. Veh. Technol.*, vol. 57, no. 4, pp. 2042-2054, Jul. 2008.

[9] A. G. Zajić and G. L. Stüber, "Three-dimensional modeling and simulation of wideband MIMO mobile-to-mobile channels," *IEEE Trans. Wireless Commun.*, vol. 8, no. 3, pp. 1260–1275, Mar. 2009.

[10] G. Acosta and M. A. Ingram, "Six time-and frequency-selective empirical channel models for vehicular wireless LANs," *IEEE Veh. Technol. Mag.*, vol. 2, no. 4, pp. 4–11, Dec. 2007.

[11] I. Sen and D. W. Matolak, "Vehicle-vehicle channel models for the 5-GHz band," *IEEE Trans. Intelligent Transportation Sys.*, vol. 9, no. 2, pp. 235–245, Jun. 2008.

[12] K. V. Mardia and P. E. Jupp, *Directional Statistics*. Chichester: John Wiley & Sons, 2000.

[13] A. Abdi, J. A. Barger, and M. Kaveh, "A parametric model for the distribution of the angle of arrival and the associated correlation function and power spectral at the mobile station," *IEEE Trans. Veh. Technol.*, vol. 51, no. 3, pp. 425–434, May 2002.

[14] X. Cheng, C.-X. Wang, D. I. Laurenson, S. Salous, and A. V. Vasilakos, "New deterministic and stochastic simulation models for non-isotropic scattering Mobile-to-mobile Rayleigh fading channels," *Wireless Commun. Mobile Computing*, accepted for publication.

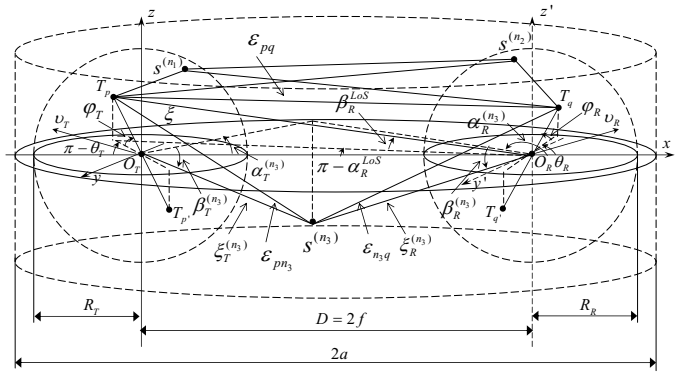

Fig. 1. The proposed 3D MIMO M2M RS-GBSM combining a two-sphere model and an elliptic-cylinder model (only showing the detailed geometry of LoS components and single-bounced rays in the elliptic-cylinder model).

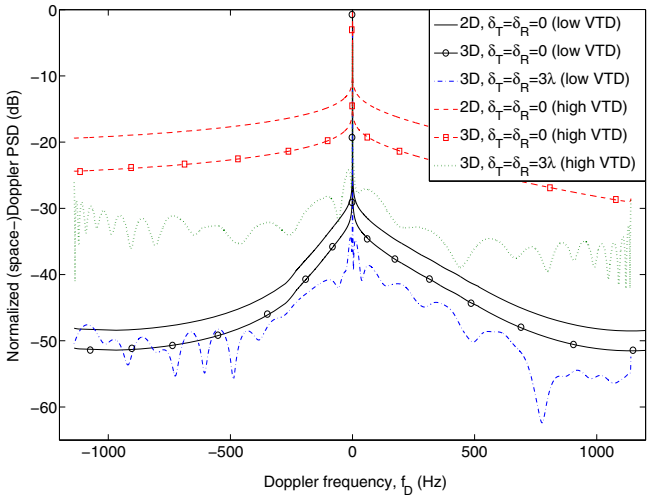

Fig. 3. Normalized (space-)Doppler PSDs for low and high VTDs.

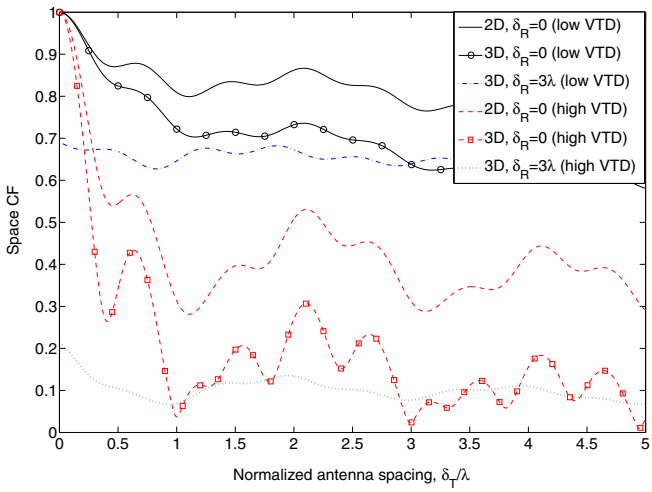

Fig. 4. Normalized space CFs for low and high VTDs.

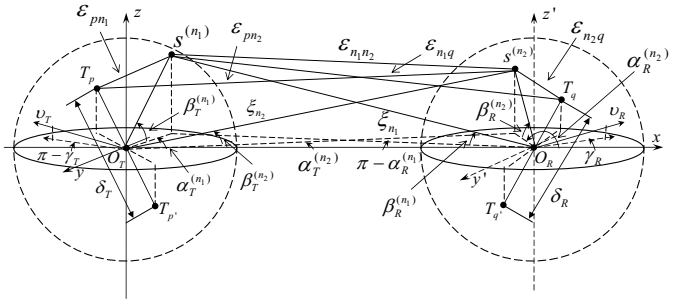

Fig. 2. The detailed geometry of the single- and double-bounced rays in the two-sphere model of the proposed 3D RS-GBSM.

TABLE I. DEFINITION OF PARAMETERS IN FIGS. 1 AND 2.

D	distance between the centers of the Tx and Rx spheres
R_T, R_R	radii of the Tx and Rx spheres, respectively
a, f	semi-major axis and half spacing between two foci of the elliptic-cylinder, respectively
δ_T, δ_R	antenna element spacings at the Tx and Rx, respectively
θ_T, θ_R	orientations of the Tx and Rx antenna arrays in the x-y plane, respectively
φ_T, φ_R	elevations of the Tx and Rx antenna arrays relative to the x-y plane, respectively
υ_T, υ_R	velocities of the Tx and Rx, respectively
γ_T, γ_R	moving directions of the Tx and Rx in the x-y plane, respectively
$\alpha_T^{(n_i)}$ $(i=1,2,3)$	azimuth angles of departure (AAoD) of the waves that impinge on the effective scatterers $s^{(n_i)}$
$\alpha_R^{(n_i)}$ $(i=1,2,3)$	azimuth angles of arrival (AAoA) of the waves traveling from the effective scatterers $s^{(n_i)}$.
$\beta_T^{(n_i)}$ $(i=1,2,3)$	elevation angles of departure (EAoD) of the waves that impinge on the effective scatterers $s^{(n_i)}$.
$\beta_R^{(n_i)}$ $(i=1,2,3)$	elevation angles of arrival (EAoA) of the waves traveling from the effective scatterers $s^{(n_i)}$.
α_R^{LoS}, β_R^{LoS}	AAoA and EAoA of the LoS paths, respectively.
ε_{pq}, ε_{pn_i} $\varepsilon_{n_1n_2}$, ε_{n_iq} ξ, $\xi_{T(R)}^{n_3}$ ξ_{n_1}, ξ_{n_2}	distances $d(T_p,T_q)$, $d\left(T_p,s^{(n_i)}\right)$, $d\left(s^{(n_1)},s^{(n_2)}\right)$, $d\left(s^{(n_i)},T_q\right)$, $d(T_p,O_R)$, $d\left(O_T(O_R),s^{(n_3)}\right)$ $d\left(s^{(n_1)},O_R\right)$, $d\left(O_T,s^{(n_2)}\right)$, respectively $(i=1,2,3)$